Carbon Monoxide Oxidation Promoted by a Highly Active Strained PdO Layer at the Surface of Au 30 Pd 70 (110)

Marie-Claire Saint-Lager, Marie-Angélique Languille, Francisco Aires, Aude Bailly, Stéphanie Garaudée, Eric Ehret, Odile Robach

Carbon Monoxide Oxidation Promoted by a Highly Active Strained PdO Layer at the Surface of $Au_{30}Pd_{70}(110)$

Marie-Claire SAINT-LAGER*[1], Marie-Angélique LANGUILLE[2,3], Francisco J. CADETE SANTOS AIRES[2,4], Aude BAILLY[1], Stéphanie GARAUDEE[1], Eric EHRET[2] and Odile ROBACH[5,6]

[1] *CNRS Institut Néel and Université Grenoble Alpes, 38000 Grenoble, France*

[2] *Univ. Lyon, Université Claude Bernard Lyon 1, CNRS, IRCELYON – UMR 5256, 69626 Villeurbanne, France.*

[3] *Present address : Sorbonne Universités, Muséum National d'Histoire Naturelle, Ministère de la Culture et de la Communication, CNRS, 75005 Paris, France.*

[4] *Laboratory for Catalytic Research, National Research Tomsk State University, 634050 Tomsk, Russia.*

[5] *Univ. Grenoble Alpes, CEA, INAC-MEM, 38000 Grenoble, France.*

*e-mail : marie-claire.saint-lager@neel.cnrs.fr

phone : (+33) 4 76 88 74 15

Abstract

Grazing Incidence X-ray diffraction and mass spectrometry were coupled to study the $Au_{30}Pd_{70}$(110) surface and correlate the depth profile of its structure to its catalytic properties for carbon monoxide (CO) oxidation, under oxygen rich conditions and at moderate temperatures (300 to 470 K). Under increasing pressure from ultra-high temperature up to 100 mbar, both pure oxygen and pure CO induce Pd segregation, even at room temperature. However, pure oxygen reorganizes the surface with a (1x2) missing row reconstruction, whereas in pure CO it is strongly roughened. These surface states evolve under higher pressure of oxygen or under CO + O_2 mixture, with a O_2/CO pressure ratio higher than a critical value depending on the temperature. It appears a phase corresponding to the initial step of the oxidation with oxygen dissolution in the subsurface region. From about 400 K, an oxidized pure Pd layer (is formed growing in the $[100]_{PdO}$ direction. This PdO phase is strained and does not coincide with the $P4_2/mmc$ structure usually observed for this oxide under ambient conditions. It is rather consistent with the high pressure I4/mmm PdO structure strained by epitaxy on the underneath alloy and would relax to the usual PdO structure for higher oxidizing conditions and layer thickness. This strained oxide is easily reduced by CO and its presence is correlated to a very high activity for CO oxidation with a performance at 470 K comparable to that found on surfaces of pure palladium at higher temperatures. The CO oxidation follows the Langmuir-Hinshelwood mechanism with a rate controlled by the CO adsorption. This work paves the way to a better understanding of the mechanism of the CO oxidation reaction on pure palladium surfaces.

Introduction

Studies on gold based alloys were stimulated by the pioneering work of Haruta *et al* showing the low-temperature carbon monoxide (CO) oxidation catalyzed by Au nanoparticles (NPs) supported on oxides.[1] The key step for CO oxidation is the O_2 dissociation since large Au NPs as well as bulk Au adsorb CO under reaction conditions but do not activate molecular oxygen.[2] Also the synergetic interaction between the NPs and the substrate was very early established.[3] More recently it has been shown that the active sites for CO oxidation on Au/TiO_2 catalysts are located at the Au-substrate interface, with O_2 dissociation occurring at a dual Ti-Au site.[4] Moreover, the geometry of the site could also plays a major role as shown by a study[5] which correlated the maximum in catalytic activity observed for particle size around 2 nm[6, 7] to the optimum of particular sites at the perimeter of the NP/TiO_2 interface. In any case the conversion rate is as low as a few CO molecules per second and per Au atom.

Alloying gold with another metal such as palladium could be another promising route for low temperature CO oxidation reaction since it adds to the gold surface an element capable of dissociating O_2. Indeed Pd is known to dissociate O_2 for temperature as low as ~150 K. But, due to the CO inhibition, pure Pd only catalyzes CO oxidation at much higher temperatures, [8] at least 450 K under steady-state conditions.[9] It was shown that PdAu(100) was much more active than pure palladium surfaces for CO oxidation around 400 K.[10,11,12,13] In ultra-high vacuum (UHV), the topmost layer of Au-Pd alloys is heavily enriched in gold even for high palladium concentration.[14,15,16,17,18,19] Under CO oxidation conditions, palladium, that forms stronger bonds with oxygen and CO compared to gold, segregates towards the surface. This segregation yields a mixed composition of the AuPd(100) surface with contiguous Pd ensembles (at least Pd dimers) required to achieve its high activity for CO oxidation.[11] But the key of the improvement of the catalytic activity would lie in the reduction of the binding energy of CO with AuPd(100) compared to pure Pd. This would facilitate CO desorption even near room temperature avoiding CO poisoning.[10]

Such Au-Pd synergy improving catalytic properties was not always observed. For instance, in the case of Au-Pd bimetallic NPs supported on TiO_2, Pd segregation was also evidenced under O_2 and O_2/CO with the formation of Au_{core}-Pd_{shell} structure.[20] However no significant improvement of the gold catalytic activity was observed. This was attributed to the possible

replacement of Au by Pd atoms in low coordination sites, which would be at the origin of the high activity in CO oxidation of the supported gold NPs.

This illustrates how the Au-Pd synergetic effect strongly depends on the system. In previous works, we studied the (110) surface of $Au_{30}Pd_{70}$ alloy and showed that Pd segregation occurs under pure oxygen and also pure CO pressure even at room temperature.[18,19] From 420 K under near ambient pressure of oxygen, an oxidized pure Pd layer grew in the $[100]_{PdO}$ direction. This PdO layer is strained and its structure was not completely solved. Such unusual palladium phase can exhibit interesting catalytic properties.

Indeed, the mechanism of the CO oxidation proceeding on Pt-group metal surfaces such as Pd is still debated even if it has been extensively studied as a prototypical catalytic reaction. In the past, it was concluded that the CO oxidation reaction proceeds via the Langmuir−Hinshelwood mechanism, whereby co-adsorbed CO and O atoms react to form CO_2.[8] The improvement of surface science techniques enables to overcome the "pressure-gap" to conduct studies in near-ambient pressure conditions on model catalysts. It led to new insights, raising questions on the reaction mechanism and on the active sites. Some of these studies found a close relationship between the existence of the oxide species and the catalytic activity, and hence suggest a Mars−van Krevelen reaction mechanism.[21] In this case, oxide species are formed on the metal substrate and control the reaction.[22,23,24] In contrast, Goodman and co-workers suggest that the most reactive surface is covered by chemisorbed O (not an oxide phase) with undetectable amounts of CO.[25,26,27,28]

The purpose of this article is to study the strained PdO phase that grows on $Au_{30}Pd_{70}(110)$ under high oxidizing conditions. We thus follow the surface structure and composition using X-ray scattering coupled with mass spectrometry, complemented by Auger spectroscopy, under increasing oxygen and CO pressures. The explored temperature range was limited to moderate temperatures, between 300 and 470 K, where most of the crucial effects regarding the catalytic properties of Pd and Pd-Au systems were observed.

Experiment

The experimental setup consists of an UHV preparation chamber coupled to a batch reactor to allow sample transfer in UHV conditions. The reactor works from UHV to reactive conditions at ambient pressures and makes possible both Grazing Incidence X-ray Diffraction (GIXRD) and

activity measurements in static conditions. It is described in details elsewhere,[29,19] only the relevant features are recalled here. The sample preparation can be performed in the reactor since it is equipped with an ion gun and a sample heating stage. The sample heating is supplied by a high-power fiber-coupled laser diode to avoid hot filament which could be responsible for undesirable reaction under reactive gases. For the same reason, the temperature was measured with an external infrared pyrometer (Impac IPE 140 MB 10). The laser source being controlled by the IR pyrometer, surface heating produced by the exothermic CO oxidation reaction is thus immediately compensated by a decrease of the power supplied. Auger Electron Spectroscopy (AES) measurements and low energy electron diffraction (LEED) were conducted in the UHV chamber by using a SPECTALEED apparatus from Omicron technology. The reactor chamber is connected to a gas manifold. A great care was taken with the gas purity and the chemical passivity of the sample environment in the reactor. N55 oxygen and N37 CO gas purity were used. Moreover, a Cu-pellet heating trap was installed on the CO gas line to avoid any metal carbonyl and moisture. The reactor gas composition was monitored by a quadrupole mass spectrometer mounted behind a CF40 gate valve. For pressures higher than 10^{-6} mbar, the reactants and products are sampled through a leak valve. The CO and CO_2 partial pressures in the reactor chamber are deduced from the 28 and 44 m/e ionization currents.

The setup is usually settled in our laboratory allowing studies on the sample preparation and low pressure characterization by LEED and Auger in the UHV chamber and reactivity measurements in the reactor chamber. Such studies can be done prior to the allocated beam time at the European Synchrotron Radiation Facility (ESRF) and after them to perform complementary measurements. The whole setup can be moved and installed at ESRF on beamline BM32 to carry out X-ray measurements from UHV up to near ambient pressure of reactive gases.[29]

GIXRD was performed with a photon energy of 18 keV, the incidence angle with respect to the sample surface being 0.3°, i.e. about twice the critical angle for a better stability during sample heating. The detector was a standard NaI scintillator. The crystal basis **($\mathbf{a_1}$, $\mathbf{a_2}$, $\mathbf{a_3}$)** used to describe the (*HKL*) directions is expressed in terms of the cubic $Au_{30}Pd_{70}$ lattice with $\mathbf{a_1}=1/2[-110]_c$ and $\mathbf{a_2}=[001]_C$ lying in the surface plane and $\mathbf{a_3}=1/2[110]_C$ out-of-plane, the *c* subscript indicates that the directions are indexed in the cubic frame. In this basis $\alpha=\beta=\gamma=90°$,

$a_1 = a_3 = a_0/\sqrt{2}$ and $a_2 = a_0$; a_0 = 3.942Å is the cubic $Au_{30}Pd_{70}$ lattice constant.[19] This unit cell is tetragonal centered and the Bragg peaks appear for even values of *H+K+L*. Unless otherwise mentioned, the indices *H, K* and *L*, in reciprocal space lattice unit (r.l.u) of the $Au_{30}Pd_{70}$(110) surface frame, will be used.

The surface was monitored in various environments by recording the diffracted intensity along mainly two kinds of scans: radial scans along *K* or *H* parallel to the surface at *L*=0.05 and two *L*-scans perpendicularly to the surface along the *(HK)* crystal truncation rods (CTR), the first being the reflectivity (*H=K=*0) the second one along the (01) CTR.

The reflectivity was measured in the so-called θ-2θ geometry from which was extracted the structure factor along the (00) CTR with the usual corrections. In this case the structure factor is not sensitive to the lateral in-plane position of the atoms but only to the mean electronic density perpendicularly to the surface. The latter depends on the composition of each atomic plane and the inter-planar distances which can deviate from their values in the bulk alloy. Since only a small region around the reciprocal space origin was explored (scattering vector close to zero), the atomic scattering factor of each element can be approximated by their atomic number Z, which is 8, 46 and 79 for oxygen, palladium and gold, respectively. To describe the occupancy per plane, we define a mean atomic number <z> normalized to that of palladium. It gives 1 for pure Pd plane, 1.7 for a pure Au plane and 1.2 for $Au_{30}Pd_{70}$, assuming in any case the same lattice parameters as the alloy.

Regarding the (01) CTRs, the correction was empirically calculated by comparing, for the same surface, the intensity along it, after background subtraction, to the (01) CTR obtained by integrating azimuthal scans following the usual ANAROD procedure.[30,31] This data reduction gives the structure factor, from which the structural parameters were deduced by fitting using the ROD software. In this case only the atoms in registry with the underneath bulk alloy contribute to its signal. Since the scattering vector along the (01) CTR cannot be neglected and the atomic scattering factor changes differently for each element, the gold and palladium concentrations were fitted for each atomic plane. For comparison we also use the mean atomic number <z> as defined just above, to represent the composition of each plane.

The set of CTRs being small, the number of fitted values was kept as low as possible. To get good fits, we thus add only one adjustable parameter, namely the roughness β.[32] It is an

oversimplified approximation of all kinds of disorders in the surface layer: interface roughness, static in-plane and out-of-plane disorders that can differ for each plane. Such an X-ray analysis, complemented by the Auger spectroscopy, allows to provide a good evaluation of the depth profile at each step of the alloy surface evolution under reactive gases in particular the number of atomic layers modified by the gas exposure, the variation of the electronic density in these planes relatively to the underneath alloy, as well as their displacement from the mean inter-planar spacing.

A clean $Au_{30}Pd_{70}$(110) surface is prepared by repeated cycles of ion sputtering (argon pressure $\approx 10^{-6}$ mbar, 2 keV) and annealing at 750 K for which the gold segregation occurs due to the difference of surface energy of Au and Pd. AES analysis shows that the ratio, $R_{Au/Pd}$ of the peak to peak height of 69 eV Au (NVV) transition on that of the 327 eV (MNN) Pd is 4.3 ±0.2. We detected no trace of sulfur peak at 152 eV, the most frequent pollutant of the AuPd alloys. Regarding X-ray measurements the surface quality was checked by the (0 1 0.05) surface peak. The width along the *K* direction is 0.034±0.002 and the angular width in the perpendicular direction is 0.63±0.03°. Its maximum intensity is referred as 10^4 counts in arbitrary units.

Experimental results

Evolution under increasing pure oxygen pressure (UHV up to 500 mbar)

The clean $Au_{30}Pd_{70}$(110) surface was first exposed to pure oxygen pressure at room temperature (RT) following a procedure detailed in figure 1 (negative side of the horizontal time axis). The surface evolves through different phases as identified in our previous work[19] and illustrated by the *K*-scans of figure 2. In UHV, the clean surface is (1x1) (see the left insert of figure1) and exhibits an intense surface peak at (0 1 0.05). When 2 mbar of oxygen are introduced, this peak rapidly decreases while a broad peak grows at *K*=1.50±0.01. It is the signature of the (1x2) missing-row reconstruction induced by oxygen adsorption, schematically represented in the second insert of figure 1 and studied in detail in elsewhere. [19] After a long exposure to the same O_2 pressure, the diffracted peaks begin to vanish. Then the O_2 pressure was increased up to 500 mbar, this provokes the reappearance of a small surface peak at *K*=1 pointed by the orange arrow in figure 1 and highlighted by its *K*-scan plotted with the same color in figure 2. It disappears when the temperature is increased to 420K and a new sharp diffraction signal rises at *K*= 1.47 corresponding to PdO. At the same

time, the gold signal disappears from AES spectra, lonely the Pd signature is observed (figure 3) showing that the surface layer becomes purely composed of palladium.

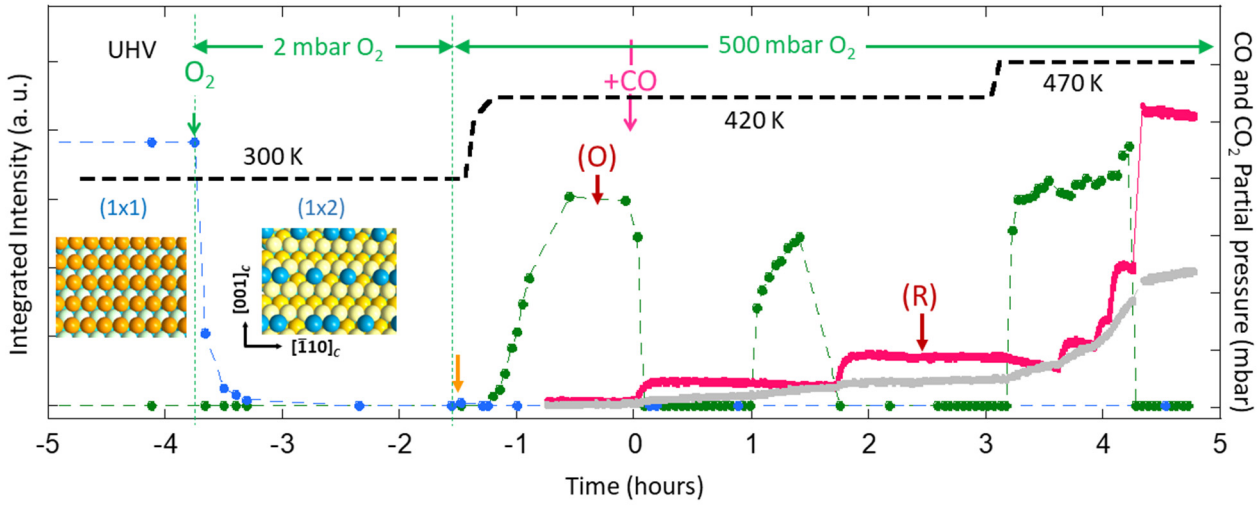

Figure 1 : *Variation induced by increasing pressure (oxygen and then CO) and temperature over time on the integrated intensity of the (0 1 0.05) surface peak (in blue) and of the (0 1.47 0.05) oxide peak (in dark green), on the partial pressure of CO (in pink) and of the produced CO_2 (in grey); blue and green dashed lines are guide for eyes. The black dashed line indicates the temperature level. A pressure of 2 mbar of oxygen is first introduced at time -3.75h (small green vertical arrow) and it is then increased to 500 mbar (at time -1.5h), the pink vertical arrow indicates the first CO introduction (at time 0h), the following jumps in the CO pressure correspond to new CO additions. The two inserts are schematic representations of the (1x1) and (1x2) $Au_{30}Pd_{70}$(110) surfaces with the typical close packed rows of the (110) face of the face-centered cubic structure along $[-1\ 1\ 0]_C$. (see more detail in ref. 19), The orange arrow points to the reappearance of the surface peak at K=1 and the two red arrows when the data were recorded on oxidized (O) and reduced (R) surfaces for X-ray analysis reported in figure 5.*

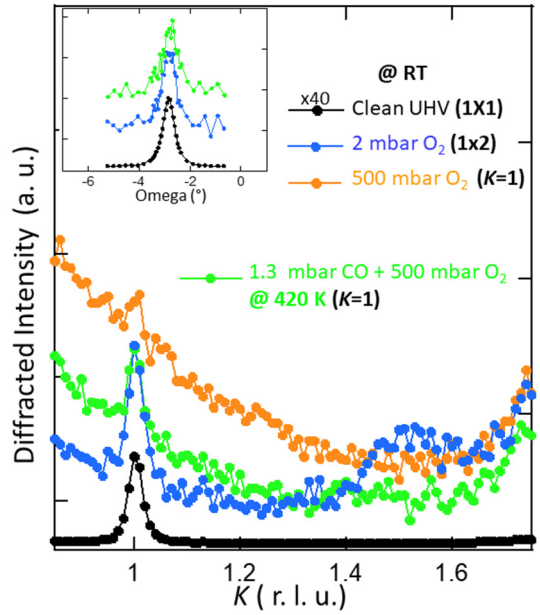

Figure 2 : *K-scan at H=0 and L=0.05 in various conditions when a small diffraction signal is detected at K=1, with, in insert, the corresponding omega scan at K=1; for the clean surface (UHV-RT curves) the intensity scale has to be multiplied by 40. We notice the increase of the background at low K when pressure increases which is due to the X-ray diffusion by gas in the chamber.*

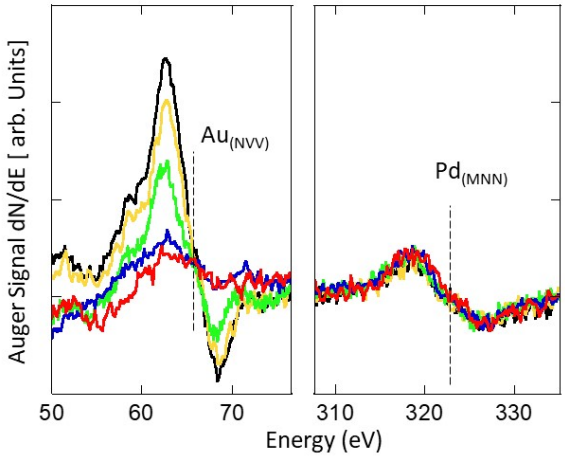

Figure 3 *: Evolution of the Auger spectra as a function of the exposure to gas : (Black) Clean (1x1) $Au_{30}Pd_{70}$(1 1 0) surface in UHV, $R_{Au/Pd}$ = 4.3±0.2; (yellow) (1x2) surface induced by 2.10^{-6} mbar oxygen at 500K, $R_{Au/Pd}$ = 3.7±0.2; (Green) post mortem in UHV , after exposure to 2 mbar oxygen at 420 K inducing a small peak at K=1, $R_{Au/Pd}$ = 2.4±0.2; (Red) after 1 mbar CO + 500 mbar O_2 at 470K on oxidized surface (sharp peak at K=1.47), (Blue) after 100 mbar oxygen + 2 mbar CO at 420K on the reduced surface (no peak at K=1.47). In these two last cases, also recorded post-mortem, $R_{Au/Pd} \sim 0$. For each curve, the intensity is normalized to the peak-to-peak height of the $Pd_{(MNN)}$ transition.*

Characterization of the thin strained oxide layer under oxygen pressure

As shown in our previous work, [19] in presence of the PdO phase, the detected diffraction peaks are at fractional values of *H*, *K*, and *L* and can be related to the tetragonal lattice of bulk PdO. The oxide grows in the $[100]_{PdO}$ direction, with the long axis perpendicular to the closed packed $[-1\ 1\ 0]_C$ rows of the $Au_{30}Pd_{70}(1\ 1\ 0)$ surface as drawn in the insert of figure 4 . The relation between the oxide Miller indices *h,k,l* with H, K, L defined in the $Au_{30}Pd_{70}(110)$ surface are : $h=0.95L$, $k=0.93H$ and $l=0.73K$. This leads to the following parameters for the PdO layer unit cell, with orthogonal axes: $a_{oxi}=2.93\pm 0.03$ Å, $b_{oxi}=3.00 \pm 0.05$ Å and $c_{oxi}=5.39\pm 0.01$ Å. The lattice parameter is contracted perpendicularly to the surface and the structure is no longer exactly tetragonal as the usual bulk PdO oxide. More remarkably we also observed small peaks at $(0 \pm 0.73\ 0.05) \equiv (001)_{PdO}$ forbidden in the usual phase of PdO. We will discuss further the structure of this PdO strained phase.

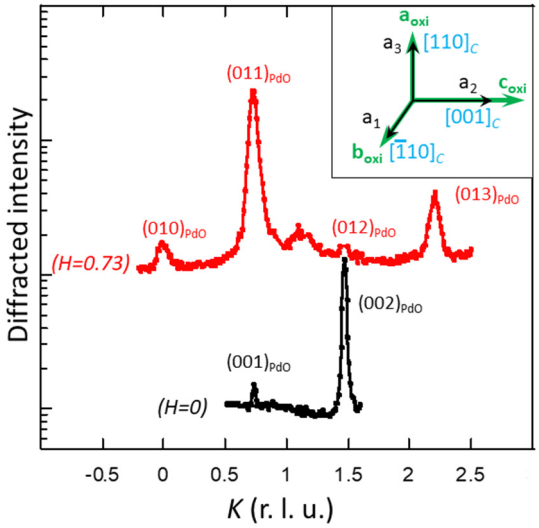

Figure 4 *: PdO peaks measured along K-scans at L=0.05, with H=0 in black and H=0.73 in red. The oxide peaks are labeled* $(hkl)_{PdO}$ *with the Miller indices corresponding to the PdO frame basis* (a_{oxi}, b_{oxi}, c_{oxi}). *The insert shows the relation between the oxide basis in green, the axes of the* $Au_{30}Pd_{70}(110)$ *surface frame* (***a_1, a_2, a_3***) - defining the H,K,L indices- in black and the directions of the cubic lattice of the alloy (in blue with the subscript c).*

One of the particularity of this oxide layer is its narrow thickness. In order to get a depth

profile of the surface layer, the reflectivity (specular rod (00)) and the non-specular (0 1) one were recorded (at point (O) in figure 1) and analyzed. The structure factor along these two rods is plotted in figure 5a and 5b (red and yellow curves). The (00) CTR presents oscillations characteristic of a fairly well defined interface between the bulk and the surface layer. Figure 5c shows the mean <z> deduced from fitting the (0 0) CTR for each atomic plane. In the topmost planes, <z> = 0.8, it corresponds to the value calculated for PdO taking into account its larger surface unit cell compared to the alloy. The displacements Δd relatively to the bulk alloy interplane distance are plotted on the same figure; it is about +6.5 % in the topmost planes, close to the PdO value. The mean thickness of this PdO layer is about 7 planes. For the deepest planes, <z>~1.2 and Δd~0 corresponding to the bulk alloy parameters, in between there is an interface layer made of 3 gold-enriched planes.

As seen by comparing the red and the yellow curves, in figure 5b and figure 5a, respectively, oscillations along the (01) CTR are much larger than on (00), involving a smaller number of planes. The Pd and Au concentrations and the interplane distances were also deduced and plotted in figure 5c. It shows a good match between the parameters deduced from the (01) CTR for the 3 planes at the interface between the PdO surface layer and the bulk alloy and those deduced from the (00) CTR. In this interface layer, in registry with the bulk alloy, the deepest plane is gold-enriched and the gold concentration rapidly decreases in the planes above.

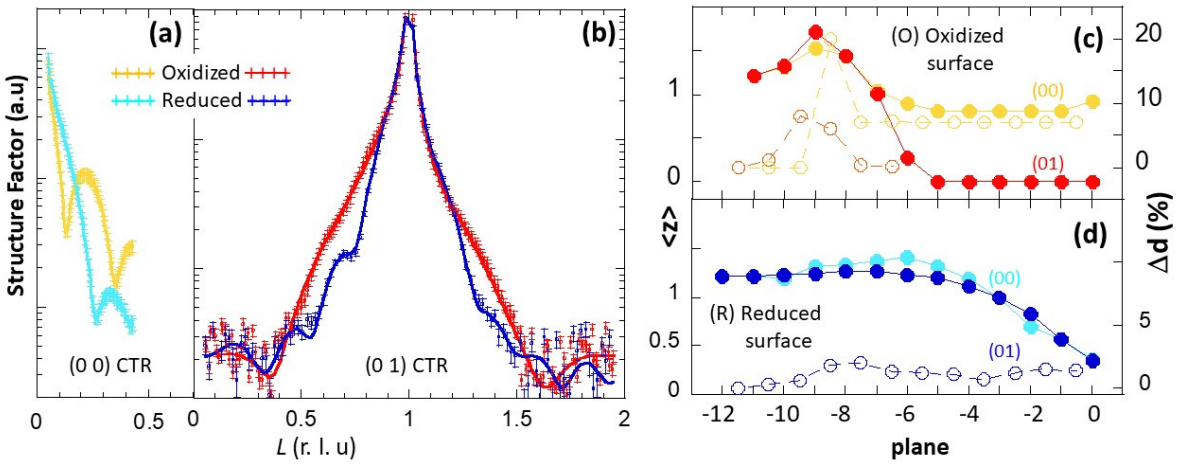

Figure 5 *: Structure factor along (a) the (00) CTR and (b) the (01) CTR , points are data and full lines correspond to the calculated values with the parameters plotted with the same color in (c) and (d) for oxidized and reduced surface, respectively. In (c) and (d) filled circles represent the mean atomic*

number <z> (left vertical axis) and empty ones the relative variation Δd compared to the bulk alloy value (right vertical axis). The horizontal axis is the number of the plane, zero being the surface plane.

For (01) CTR, the best fit was obtained for a large β=0.7. The (01) signal coming from the buried layer, the high value indicates that this layer is not well organized with only a fraction of atoms in registry with the bulk underneath.

Behavior of the PdO strained phase in reactive mixture CO + oxygen

Reducing of the PdO layer by CO

To check the reactivity of the present PdO layer, CO was added to 500 mbar of oxygen with progressively increasing pressure at 420 K. As shown in figure 1, 0.5 mbar CO at 420K immediately vanishes the oxide peak, it reappears one hour later but disappears again at the moment of a new introduction of 0.5 mbar CO. The oxide peak rises again when heating the sample at 470K and stays stable up to a CO partial pressure of about 10 mbar which makes the oxide peak vanish again. Auger spectra performed on such reduced surface show that, as for oxidized one, the topmost planes are purely composed of palladium (figure 3).

As previously done for the surface oxide, the (00) and the (01) CTRs were recorded and analyzed in the stage where the oxide peak disappeared (Point(R) in figure 1). The results are also reported in figure 5 together with those of the oxide surface evidencing their quite different behavior. If we compare the blue curves of figure 5a and 5b, we see that, the oscillations on the (00) CTR of the reduced surface are larger compared to the oxidized surface and, interestingly, they have roughly the same frequency as on the corresponding (01) CTR. This means that the structure has strongly changed. The oxide layer was replaced by a layer with atoms mainly in registry with the bulk alloy. The best fit of the (01) CTR was obtained for roughness parameter a bit smaller than for the oxidized surface (β = 0.5 instead of 0.7). The <z> values as deduced from the (00) and (01) CTRs, plotted in figure 5d, follow the same trends; they have about the bulk alloy value for the deepest planes and drop below the palladium value when approaching the surface. Since this lowering is similar for the (00) and the (01) CTRs, it cannot be attributed to the disorder but rather to a decrease of the occupancy when approaching the surface. It implies that the height of the layer is irregular. Moreover, importantly it shows that the surface layer structure is uniform, in particular this precludes

the presence of another phase such as powder-like PdO which would contribute to the reflectivity but not to the (01) CTR.

Regarding the inter-planar spacing, there is a tendency to a small expansion compared to the bulk alloy with an average value of 1.3 %; it corresponds to + 2% compared to bulk palladium.

Reactivity of the oxide phase

Figure 1 also evidences the remarkable correlation between CO and Pd oxidation. The presence of the oxide peak at (0 1.47 0.05) is systematically accompanied with an acceleration of the CO conversion into CO_2. When CO is added to 500 mbar of O_2 at 420K, no reaction is observed and the oxide peak disappears. When it reappears, after a long delay, we detect a small rate of CO conversion into CO_2, the pressure ratio O_2/CO being about 1000. The conversion rate sharply slowed down with a new CO introduction correlated with the vanishing of the oxide peak.

When the sample is heated at 470 K, CO oxidation accelerates again and is accompanied by the comeback of the oxide peak. Increasing the pressure provokes an increase of the CO conversion rate. But a total CO partial pressure of about 10 mbar, decreasing the pressure ratio O_2/CO down to 50, makes the oxide peak vanish again and heavily slows down the rate of the CO oxidation reaction.

At each temperature, two regimes can be distinguished: one with a low reaction rate and one with a high reaction rate. The low reaction rate regime corresponds to diffraction spectra with no oxide peak that was characterized as a reduced surface. To determine the conversion rate catalyzed by the sample surface itself, we estimated the environment contribution by doing an experiment with no sample. It gave a sample environment contribution negligible at 300K but which significantly increased with temperature. We evaluated its rate as if it was produced by a surface equivalent to the sample one, one site been one surface atom. We found 5 CO_2 molecules/s/site at 420K, and 100 CO_2 molecules/s/site at 470K. In any case, the rate was comparable to that measured in the low activity regime, which is thus below the accuracy of our measurements.

The high reactive regime occurs when the surface alloy is oxidized. The O_2/CO pressure ratio ranges in a small area around 1000 at 420K and from 500 to 50 at 470K. The CO conversion rates into CO_2 obtained at 470K in several conditions were put together in figure 6 as a function of the CO partial pressure added to a constant oxygen pressure of 500 mbar. This

rate is proportional to the CO pressure up to 10 mbar. It is equal to 500 molecules per second and per surface atom for 5 mbar of CO (O_2/CO=100). Figure 6 also shows that the measured value for pure Pd(110) is on the same curve. Since this measurement was performed in the laboratory, with the same set-up, but without X-ray characterization, we were not able to verify if this pure palladium surface is oxidized or not. Anyway, the fact that the alloy surface behaves as the pure Pd one is not surprising since we have seen by Auger spectroscopy that it corresponds to pure Pd within the experimental conditions used.

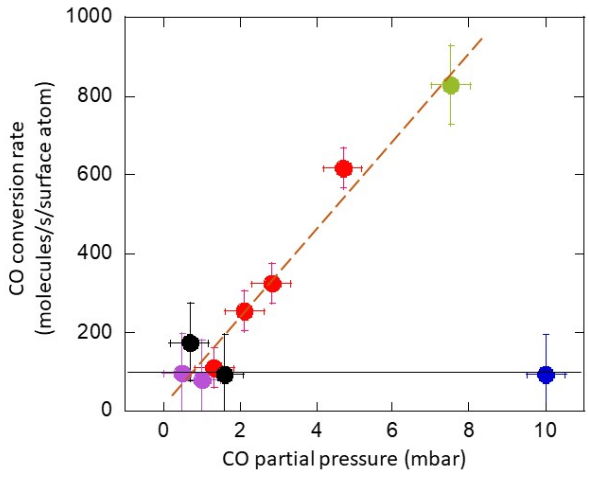

Figure 6 : *CO conversion rate into CO_2 measured at 470K as a function of the CO pressure added to 500 mbar O_2 on $Au_{30}Pd_{70}$(110) oxidized surface (in red) and reduced surface (in blue), on Pd(110) surface (in green) and on the sample holder (in black). The purple points were obtained for CO introduced before oxygen (see fig. 9a). The CO conversion rate was calculated assuming that only the free surface of the sample is active. The black horizontal line indicates the background level due to the sample environment.*

PdO surface phase formation with CO

The formation of this oxide phase was then studied under mixed pressure of CO and oxygen. For that purpose the clean surface was directly exposed to CO at room temperature. The surface, as well as the gas composition in the reactor, were followed when adding oxygen and increasing the temperature (figure 7). The reflectivity and (01) *L*-scan were recorded at several steps of this evolution marked by stars. The mean <z> per plane deduced from fitting of the (01) CTR is plotted in figure 8c.

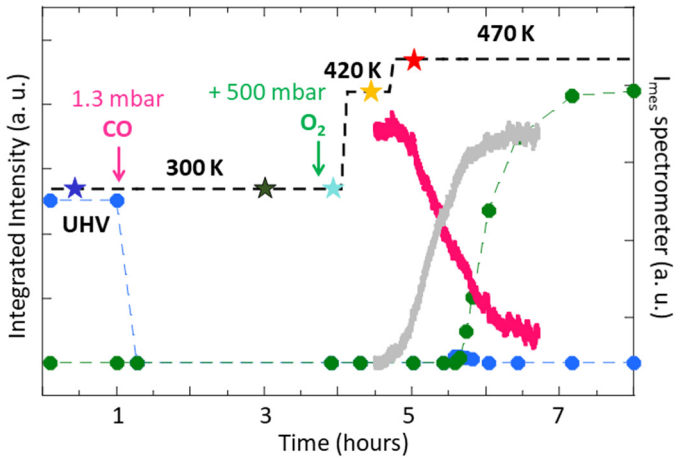

Figure 7 : *Variation induced by increasing pressure (CO and then oxygen) and temperature over time with the same code as in figure 1: integrated intensity of the (0 1 0.05) surface peak (in blue) and of the (0 1.47 0.05) oxide peak (in dark green), CO partial pressure (in pink) and produced CO_2 (in grey); blue and green dashed lines are guide for eyes. The pink arrow indicates the introduction of 1.3 mbar of CO at RT on the clean surface and the green one the adding of 500 mbar of oxygen (at RT). The stars on the black dashed line of the temperature indicate the time when the L-scans, plotted with the same color in figure 8, were recorded.*

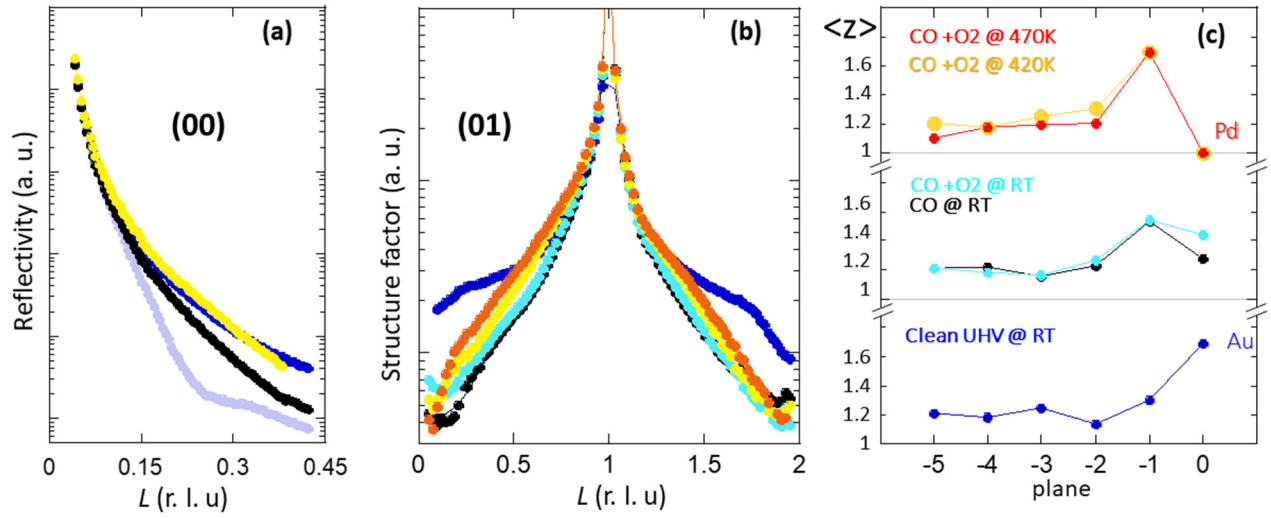

Figure 8 **:** *(a) Reflectivity and (b) (01) CTRs with the same color as the stars of figures 7 (and 9a for the light purple curve in (a)), indicating when they were recorded; points being experimental data and lines corresponding to fits; the corresponding mean atomic numbers <z> for each plane are drawn in (c).*

CO pressure immediately destroys the (0 1 0.05) surface peak of the UHV clean (1x1) surface as seen in figure 7. Figures 8a and 8b show that the reflectivity and the (01) CTR intensity (black curve) are significantly lowered compared to that measured in UHV (dark blue curve).

The CTR analysis indicates that the CO pressure at room temperature favors Pd enrichment of the surface plane and an increase of the roughness parameter β (from 0.2 to 0.6), consistently with STM results already published.[18] The surface plane composition was evaluated to be about half gold and half Pd (dark curve in fig. 8c).

When 500 mbar of oxygen is added at room temperature, there is no noticeable change of the surface structure (see light blue curves in figure 8b and 8c). Increasing the temperature to 420 K does not induce CO oxidation reaction but the roughness decreases (β = 0.4) and accelerates the trend observed at RT with Pd segregation yielding a surface plane of almost pure palladium and a second plane very rich in gold (see yellow curves in figure 8b and 8c).
When heating at 470 K, the CO oxidation started but it is not correlated to a change in the CTR (red curve of fig. 8c). However the conversion rate, calculated in this case and reported in figure 6 is comparable to the sample environment contribution. This is highlighted in figure 9a where the CO and the CO_2 signal are plotted with scales corresponding to that of figure 1. It means that if the surface contributes to the CO oxidation, its rate stays too low to be extracted from the background. Anyway, this CO conversion lowers its partial pressure in the reactor and thus increases the ratio O_2/CO yielding the conditions for the oxide formation. When, at least three quarters of CO are converted into CO_2, the PdO peak begins to gradually rise as seen in figure 8a. It should be noted that this corresponds to an O_2/CO pressure ratio of about 1500.

Figure 9a allows to follow in more detail the oxide formation occurring 1 hour after the temperature reached 470K. In this zoom, the surface peak intensity, which reappears after being vanished by the initial CO introduction, has been multiplied by 40. This short reappearance acts as the precursor signal of structural transition to palladium oxide. Before the surface evolution was weak and the main changes induced by the reactive gases were localized in the 2 topmost planes, including the step marked by the red star at the beginning of the temperature plateau at 470K. The corresponding mean <z> is plotted on the bottom curve of figure 9c together with that of the green curve recorded just at the beginning of the reappearance, the oxide peak being still zero. This latter indicates the gold segregation towards the alloy with a decrease of its concentration in the second plane and an increase in the third one, while palladium segregation evolves in the opposite direction. In the same time, we found a tendency to an increase of the inter-planar spacing $\Delta d_{-1,0}$ and $\Delta d_{-2,-1}$, even if the

gold concentration has decreased. This can be attributed to oxygen insertion in the second plane (plane -1).

Even before the disappearance of the small surface peak, the oxide peak at (0 1.47 0) begins to slowly grow. The reflectivity was recorded just when the surface peak vanishes again, the oxide peak being at about 40 % of its maximum value (purple star on figure 9a). The oxide thickness is about 3 planes. The (01) CTR was recorded 15 minutes later (dark purple star) and its behavior is similar to what was observed for oxidation under pure oxygen (figure 5). However the oscillations are less pronounced corresponding to the vanishing of the gold rich interface layer between the alloy and the oxide.

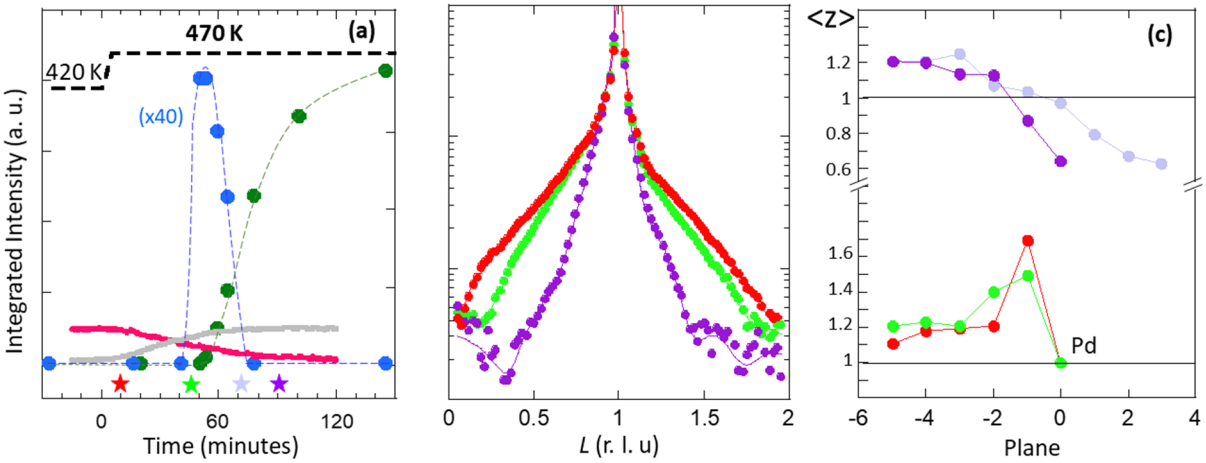

***Figure 9** : (a) Zoom on the beginning of the oxide peak formation under 1 mbar CO + 500 mbar O_2, time 0 being taken at the beginning of the heating at 470K , the labels are the same as in figure 7 but with surface peak intensity (in blue) multiplied by 40 and the scale of CO and CO_2 signals is adjusted such as their evolution can be compared to that of figure 1. As in figure 7, the stars indicate the time where the (01) CTRs, plotted in (b) were recorded, the corresponding <z> being drawn in (c). Red data (also shown in figure 8) represent the sample surface just after heating at 470K and the green later at the beginning of the reappearance of the surface peak, the two corresponding mean <z> are plotted in the bottom of (c). Purple data were recorded when the surface peak was vanished during the oxide growth, the deduced <z> being drawn on top of (c) with in dark purple, the values deduced from the (01) CTR and in light purple those from the reflectivity in figure 8a.*

Discussion :

Palladium segregation

As previously evidenced, while the clean surface of $Au_{30}Pd_{70}$(110) is almost pure gold, an exposure to pure CO or to pure oxygen pressure causes palladium segregation towards the surface, even at room temperature.[18,19] Under pure oxygen, the topmost plane becomes pure Pd and the two following ones are gold enriched, oxygen adsorption induces a (1x2) missing row reconstruction with regular depression every 3 Pd atoms along the remaining row.

Under pure CO pressure, the surface composition is AuPd mixed, and the gold surface atoms segregate towards the second plane. The CO effect stays localized in the very near surface region. No reconstruction was observed but a strong roughening occurs, as seen on STM images.[18] As already pointed out, for a metal surface in contact with CO, this reduces the effective step free energy and can even lead to the spontaneous formation of steps.[33,34] Increasing the temperature, after adding oxygen, reduces the roughness but increases the Pd content in the surface plane with no trace of reconstruction induced by oxygen as the (1x2) missing row. Thus the palladium surface stays probably poisoned by CO, blocking oxygen adsorption. CO desorption requires to increase the O_2/CO pressure ratio above a critical value corresponding to a given temperature (~1500 at 470K). In our batch reactor this was achieved by the CO conversion due to the sample environment.

The formation of palladium oxide is preceded by the reappearance of a small surface peak at *K*=1. Under pure oxygen it can be observed even at room temperature, but for higher pressures than those necessary for the (1x2) missing row reconstruction. X-ray analysis as well as the Auger spectra plotted in figure 3 show that it corresponds to a Pd enrichment of the surface. The palladium oxide formation requires heating to at least 420K; no trace of gold is visible on the Auger spectra showing that a pure palladium oxide layer has grown. This effect is not reversible, even when the surface is reduced, it remains purely composed of palladium.

Initial oxygen incorporation

We first focused on the stage preceding the oxide formation observed under pure oxygen at room temperature or under an O_2 + CO mixture (for a O_2/CO pressure ratio greater than 1500 at 470K) and distinguished by the reappearance of a small surface peak at *K*=1. The corresponding K-scan at *H*=0 and *L*=0.05 are plotted together with that of the (1x2) surface in

figure 2. It shows that this peak is, in all cases, very similar in intensity and in width along radial and azimuthal scans (ΔK = 0.035±0.05, $\Delta\omega$=0.7±0.1°). Moreover, these widths are close to those of the surface peak of the (1x1) clean surface even if this later is much more intense (x40). This is not the same for the (1x2) reconstruction peak at *K*=1.5 which is broader in both directions. In the case of the oxide peak, found at 1.47, its width in ΔK is similar to the surface peak but $\Delta\omega$ is larger as we will discuss later. It can be thus concluded that in any case the small (010) peak stays a surface peak, the intensity of which depends on the surface state.

Moreover as shown by the (01) *L*-scan in figures 8b and 9b, its small intensity can be attributed to its closeness to a minimum of the structure factor as expected for a layer with a thickness of 2 atomic planes. This originates from the destructive X-ray interference at this point[35] which is thus very sensitive to any change in the surface structure. The (01) CTRs analysis indicates that the atomic planes concerned by the changes induced by the gas pressure, have thickened from 2 to 3, as shown by <z> curves in the bottom of figure 9c, palladium segregated through the surface as also shown by AES spectra of figure 3. In the same time, the CTR fit shows that the inter-planar spacing on each side of the second plane is expanded. This can be explained by oxygen insertion in this plane.

Structural evidence of oxygen insertion as the initial step of Pd oxidation is very scarce.[36] This phenomenon is much more established by X-ray photoemission Spectroscopy (XPS) measurements, and seems to be specific of an induction period before the palladium oxidation for both Pd(111) and Pd(110).[37] Indeed the $P3d_{5/2}$ core level consists of three components, the bulk one at a binding energy of 334.9 eV and two oxygen induced components shifted at a higher binding energy by 1.3 eV and 0.65 eV with either four oxygen neighbors or two, respectively.[38] The latter was assigned to dissolved oxygen.[39] During this period a great amount of dissolved oxygen is localized in the near surface region, LEED and AES revealing that palladium is still in a face-centered cubic (fcc) metallic state.[40] However a different interpretation of the XPS spectra was suggested by a coupled STM, XPS and DFT study of oxide formation on Pd(110).[41] The authors used a more complicated decomposition involving the oxygen-induced reconstructions with, first, the c(2x4)-O reconstruction and then, the so-called "complex" one.[42] This later is formed by (7x$\sqrt{3}$) and (9x$\sqrt{3}$) domains in which the $[-110]_C$ Pd rows are decorated by O atoms in a zig-zag pattern as for the c(2x4)-O but with Pd filling the missing row. [41] Moreover in a further study by SXRD,[43] the authors attribute to this

"complex" structure the reappearance of the (010) peak that coincides with the very beginning of the oxide peak in a quite similar way than what we observed in figure 9a (to be compared to the figure 10a of ref. 43. In other words this "complex" structure could correspond to the structure of the surface during the step of oxygen insertion in subsurface region.

The initial incorporation of oxygen was studied by DFT for Pd(111) showing that the most stable state for a 0.75 -1 ML oxygen coverage is a coupling of oxygen adsorbed on a fcc site at the surface and oxygen inserted in tetrahedral subsurface sites.[44] However the expected metastable state must be quite different on the low dense (110) face as compared to that of the densest (111) face with an unlike geometry. Anyway it is clear that the stable oxygen adsorption site on the (110) surface are of tetrahedral type as seen for the two c(2x4)-O and "complex" reconstructions. But, in the bulk the most probable interstitial sites are the octahedral ones as already observed.[45] The two kinds of sites are represented in figures 10a and b. These octahedral holes are substantially the largest ones and, as already mentioned, no impurity has been found to occupy tetrahedral holes in bulk Pd, even hydrogen is inserted in octahedral sites.[46] As we observed the subsurface oxygen is particularly unstable since the (010) peak quickly vanished when the oxide one grew (figure 9a). Indeed, in PdO, due to its $4d^8$ electronic configuration, the Pd^{2+} ions are tetrahedral coordinated with a square planar geometry. The role of these subsurface oxygen is thus that of a metastable precursor of palladium oxide.[44]

The presence of this (010) diffraction signal indicates that oxygen dissolution can occur even at room temperature but for pressures close to the atmosphere (figure 2). However such oxygen insertion could be favored in the $Au_{30}Pd_{70}$ alloy since the lattice is slightly expanded relatively to pure Pd (+1.3 %). Anyway this behavior is consistent with what is observed on pure palladium oxidation of the (110) face since no surface oxide is formed before the formation of the PdO bulk oxide.[43] Unlike Pd(111) and Pd(100) surfaces that pass first through a two-dimensional oxide Pd_5O_4[38]or $(\sqrt{5} \times \sqrt{5})R27°$-PdO(101),[47] respectively, this latter can be represented by a monolayer of the PdO(101) surface of the usual oxide phase.[48]

No scan, passing through the (010) position, was recorded during CO oxidation reaction conditions, so we cannot conclude if this dissolution phase also occurs during the switch between the reduced to the oxidized surface. However, we have seen that, in these two

states, there is a pure layer of palladium at the surface and this switch would behave in a similar manner as for the pure Pd(110) surface.

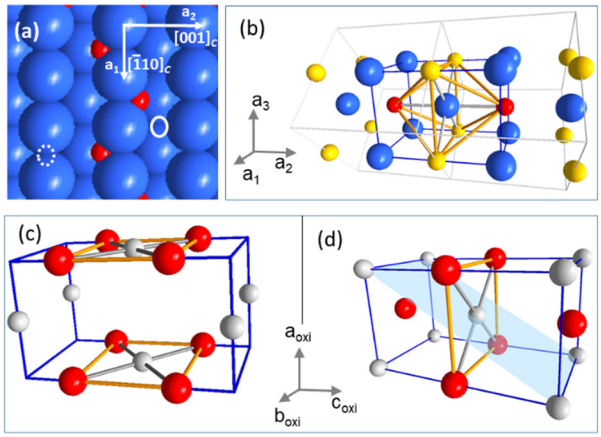

Figure 10 *: schematic of atomic arrangements in the surface layer formed with Pd under oxidizing conditions. Metallic Pd atoms are represented in blue and the* Pd^{2+} *ions in grey, oxygen atoms are in red. (a) Pd surface with adsorbed oxygen atoms in zigzag pattern in tetrahedral sites as in the c(2x4)-O and in the "complex" structure, an octahedral site is indicated by the white ellipse on the surface plane and by a dashed one for the second plane. (b) Representation of the Pd unit cell with oxygen (yellow balls) in all the available octahedral sites, those that could be filled during the dissolution in subsurface sites are in red (dashed ellipse of (a)); (a1, a2, a3) coordinates defined the surface frame of* $Au_{30}Pd_{70}$*(110) (see fig.4) . (c) Unit cell of PdO with the usual* $P4_2/mmc$ *structure and (d) unit cell of the HP I4/mmm structure; the PdO(101) plane is represented in blue. The axes are the same for (c) and (d) and are orientated as found for the PdO growth in this study (see fig. 4).*

Structure of the strained PdO phase

The oxide phase observed under 100-500 mbar of oxygen and around 420-470K, is pure Pd and has a slightly deformed tetragonal structure grown in the $[100]_{PdO}$ direction with cell parameters: a_{oxi}=2.93± 0.03 Å, b_{oxi}=3.00 ± 0.05 Å and c_{oxi}=5.39± 0.01 Å and the unit cell volume is 47± 1 $Å^3$.

The most common phase of PdO in ambient conditions is of PtS type and has the $P4/_2mmc$ structure with a=b=3.046Å and c=5.339 Å,[49] giving an unit cell volume of 50.1 $Å^3$. The PbO type

phase is also mentioned[50]but not documented.[51] Under high pressure (HP), PdO crystallizes in an I4/mmm structure which is slightly more elongated along the *c* direction, with *a*=*b*=2.982Å and *c*=5.383 Å,[52] yielding to a volume of 47.9 Å^3. These two bulk phases are represented in figures 10c and 10d. The measured parameters are slightly closer to the HP tetragonal phase with a contracted volume compared to the usual PdO phase. We can remark that this HP structure can be easily deduced from the Pd with oxygen in octahedral sites by an expansion of the basic square (from 2.75 x 2.75 Å^2 for pure Pd to 2.98 x 2.98 Å^2 for HP PdO) and a large lengthening of the long axis (from 3.89 Å to 5.383 Å) (see figure 10b and 10d). In this transformation, the oxygen atoms lose 2 of the 6 first neighbors. In the PtS phase, each metallic ion is in the center of a rectangle with oxygen atoms at the corners forming O-Pd-O angles of 82° and 98° instead of 90° in a square.

Bragg intensities

Regarding the Bragg peak intensities, in the two bulk oxide phases (fig10c and 10d), the Pd atoms are localized on the centered tetragonal lattice and give rise to intense Bragg peaks with (*h+k+l*) even. In the HP phase, oxygen atoms have the same symmetry and contribute to the same peaks as Pd. It is not the same in the LP structure where oxygen gives rise to additional peaks, with low intensity, following the rule *h* or *k* even, *h+k+l* being odd.

The most intense diffracted peaks measured for the strained palladium oxide layer correspond to the intense Bragg peaks common to the two bulk oxide phases, even if the base of the unit cell is not exactly a square as expected for a tetragonal symmetry. Otherwise the presence of small peaks found at $(010)_{PdO}$ is only consistent with the LP $P4_2/mmc$ structure where it is induced by oxygen atoms. However there are remarkable discordances, namely the appearance of a $(001)_{PdO}$ peak (cf. fig. 4) forbidden in the $P4_2/mmc$ symmetry and an overestimated value for the $(010)_{PdO}$ and $(012)_{PdO}$ allowed peaks. Indeed the expected ratio between the structure factor at $(002)_{PdO}$ and at $(010)_{PdO}$ is about 5 when the experimental values of F_{002}/F_{010} are at least twice as big (see table 1).

SAMPLE P and T conditions	Oxide Thickness (M L)	(0 0 2) 23.3 nm^{-1}		(0 0 1) 11.7 nm^{-1}			(0 1 0) 20.9 nm^{-1}		
		Δq	Δω	Δq	Δω	F_{002}/F_{001}	Δq	Δω	F_{002}/F_{010}
(1) 100 mbar O_2 @ 420 K	5 ± 1	0.55	4.7 ±0.2	0.45		11 ± 0.5	0.43	4.3 ± 0.2	9 ± 0.5
(2) 500 mbar O_2 @ 420 K	7 ± 1	0.55	6.5 ± 0.2						
(3) 1 mbar CO + 500 mbar O_2									
@470K + 80 min	3 ± 1	0.68	2.1 ± 0.1	0.54		7 ± 0.5			
+ 135 min		0.60	2.0 ± 0.1	0.45	1.9 ±0.1	9.6 ± 0.5	0.44		10.5 ±1
(3) UHV@RT (+150 min)		0.60		0.45		8.3 ± 0.5			

***Table 1** : Experimental characteristic of the $(001)_{PdO}$, $(010)_{PdO}$ and $(002)_{PdO}$ oxide Bragg peaks (given with their corresponding scattering vector, at L=0, $q=2\pi((H/a_1)^2 + (K/a_2)^2)^{½}$) measured for 3 samples in several experimental conditions: first line sample (1) oxidized under 100 mbar of pure oxygen at 420 K; second line sample (2) of figure 1 at the step indicated by the red arrow (O) and following lines sample (3) monitored in figure 7 and 9a at different steps under 1.3 mbar of CO plus 500 mbar of oxygen plus, first at minute 80 after heating to 470K and next line at minute 135; last cell line: sample(3), 150 min after pumping down UHV and cooling to RT. The ML column gives the mean PdO thickness in number of atomic planes as deduced from the (00) CTR fitting. The width Δq (in nm^{-1} and with the error bar ±0.05 in any case) and the mosaicity Δω(°) are reported for each peak; F_{002}/F_{001} and F_{002}/F_{010} are the ratio of the structure factors.*

The behavior of the two peaks $(010)_{PdO}$ and $(100)_{PdO}$ is very intriguing. They share common features with the $(002)_{PdO}$ reflection indicating that they are generated by the same PdO layer as illustrated by values in table 1 for 3 samples in different conditions. For instance, all the diffraction peaks have the same width Δω for a given sample; it corresponds thus to the oxide mosaicity. This depends significantly on the way by which the oxide was formed (oxygen pressure and temperature) varying from 2° to 6.5° but staying stable afterwards. Regarding the width of the momentum transfer, Δq, it increases from $(001)_{PdO}$ to $(002)_{PdO}$ indicating that it corresponds to a lattice gradient of ~10^{-2} and a domain size of ~20 nm in the c_{oxi} direction, perpendicular to the closed packed rows of $Au_{30}Pd_{70}(110)$. We note that during the oxide growth on sample (3), the peaks were wider in *q* at minute 80 than at minute 135; this corresponds to an increase of the coherence domain along *K* from 15 nm to 20 nm. Figure 11, that reports the evolution of $(001)_{PdO}$ and $(002)_{PdO}$ peaks while the PdO layer was growing, shows that $(001)_{PdO}$ intensity was more or less constant whereas the bulk $(002)_{PdO}$ significantly increased. This would indicate that the $(001)_{PdO}$ diffraction signal comes from the PdO layer but, more precisely, from its surface. We have less information about the $(010)_{PdO}$ diffraction

signal, but when it was measured, its structure factor had a value comparable to that of the $(001)_{PdO}$ one (see table 1) indicating that they have the same origin. This means that there is no Bragg reflection added by oxygen atoms and that the PdO structure looks like that of HP PdO I4/mmm structure. Such results can be explained since this PdO thin layer is in epitaxy on the alloy and it is well known that it is a way to synthesize unusual structures that would only appear under high pressure conditions.

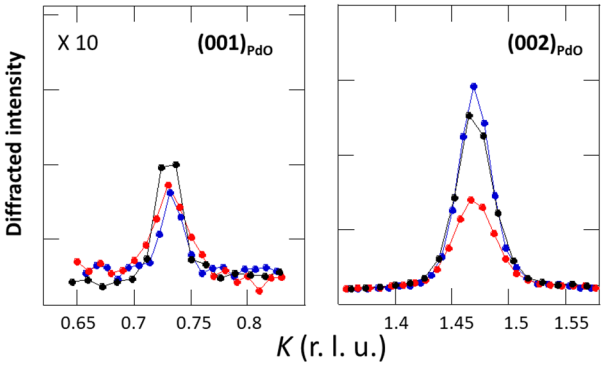

***Figure 11**: Comparison of the diffracted intensity of the (001) and (002) Bragg peaks of PdO, (blue) sample (1) under 100 mbar of pure oxygen at 420K, (red) sample (3) under a mixture of CO + O_2 at 470K and during the growth of the oxide layer corresponding to the purple star of figure 8a and (black) the same sample but after cooling to RT and pumping down to UHV.*

Comparison with PdO growth on pure Pd surfaces

A study of the growth of oxide on Pd(110) under oxygen pressure was performed by GIXRD.[43] It showed that PdO has relaxed and the $[100]_{PdO}$ axis is ~±7° tilted from the perpendicular to the Pd(110) surface. The $(001)_{PdO}$ peak can be seen in their diffraction pattern and not the $(010)_{PdO}$ ones as expected for the usual LP bulk-like PdO. This result is significantly different from the strained layer of the present work. But it was produced in more oxidizing conditions, above 0.5 mbar O_2 at 620K, namely 150 to 200K higher than in our work. This yielded diffraction peaks with a much thinner extension in the *L* direction meaning a much thicker PdO layer. A strained epitaxial PdO thin layer was already evidenced by GIXRD for Pd(100) in similar conditions of temperature.[53] In this case the oxide grows in the $(101)_{PdO}$ direction and upon further increase of the O_2 partial pressure a polycrystalline Pd oxide forms on the surface. Besides it was shown that on Pd(111) the oxide also grows in the $[101]_{PdO}$ direction.[54]

PdO surface

As seen in figure 10c and 10d , when PdO grows in the $[100]_{PdO}$ direction there is a stacking of alternatively pure Pd and PdO_2 planes in the LP structure. In UHV, none of these surfaces is stable since they are non-stoichiometric and thus belong to the class of the polarsurfaces, but under oxygen pressure the PdO_2 plane becomes the most stable termination.[55] In the HP structure, all planes are stoichiometric. Actually, the termination of the PdO layer formed on $Au_{30}Pd_{70}(110)$ cannot be deduced from the X-ray analysis, but figure 11 shows that the intensity of the Bragg peaks of the oxide formed under oxygen pressure stays stable even after pumping down to UHV. Since the layers are thin (few ML), surface changes could be expected to be reflected in these intensities. This also supports a structure of HP type. In this case, for each surface, a palladium atom is linked to 2 oxygen atoms instead of 4 in the bulk or in the surface plane of the usual PdO structure. This is consistent with XPS where the component corresponding to a Pd atom with 2 oxygen neighbors remains even when the oxide is well established.[37]The HP PdO surface is also stoichiometric for a growth in the $[001]_{PdO}$ direction but not in the $[101]_{PdO}$ one (cf. figure 10d). The $[101]_{PdO}$ growth is observed for oxidation on Pd(100) and Pd(111),[47,38] the stacking along $[101]_{PdO}$ growth axis presents an alternation of Pd and oxygen planes. Also it has been shown that for the usual PdO structure and in oxygen atmosphere the polar O-terminated could be stable.[55]

Activity of the PdO layer for CO oxidation

The reactivity of the surface of this strained PdO is quite different than the usual bulk-like one. For instance we showed that the PdO layer is instantly reduced upon exposure to 0.5 mbar of CO at 420K whereas reduction starts at higher temperature, above 500 K, for PdO bulk-like NPs[56] or deeply oxidized PdO layers.[57] Moreover we found that this strained PdO phase is systematically associated with a high CO conversion rate into CO_2. It can reach 500 CO_2 molecules/s/surface atom under 500 mbar O_2 + 5 mbar CO at 470K. Conversely, it was shown that pre-oxidized Pd(110) surface was almost unreactive for CO oxidation,[9] but such a surface was obtained under strong oxidizing conditions that is to say more than 20 minutes above 800 K and under 1 Torr of O_2.

The O_2/CO critical ratio

The presence of the strained oxide is directly linked to a high CO conversion rate into CO_2 and, moreover, the required O_2/CO ratio to obtain this active surface is similar to what was already observed.[25] It was shown that the O_2/CO ratio value, required for the appearance of the highly active phase, increases with decreasing temperature: it is around 65 at 470K and can be extrapolated to 320 at 420K. [25] Here we found, at 420 K, a small domain of existence of the active phase around 1000, but with a low reaction rate of about 5 CO_2 molecule/s/surface atom (above the background). At 470K, the high active phase was observed for O_2/CO between 500 and 50 if a pure Pd layer was already present at the surface. We point out that in the case of reaction in a batch reactor, the conversion by the sample environment may play a role. Indeed, we observed that it consumes CO and can contribute to diminish its partial pressure in the reactor and so to reach the oxide formation limit. This can explain the long delay observed for the oxide phase formation in figure 7 at 470K, but also the one observed at 420K in figure 1.

The hyperactive active regime?

However, even if the CO limits for the high active phase are similar to those found by the Goodman's group,[25] we did not evidence the "hyperactive" surface, with CO_2 formation rate more than ten times higher than the maximum of our values. This would appear as a transitory state between *(i)* a low active regime on a CO-inhibited metallic surface for low temperature and near stoichiometric O_2/CO ratio and *(ii)* a high-temperature regime where the CO_2 formation rate is either mass transfer limited on a metallic surface or limited by the reduced reactivity of the oxidized surface.[10] This hyperactive state was evidenced in a batch reactor, as in our experiments, but it had a very short lifetime (a few seconds) that we cannot measure. Moreover, it is now known that during the transition state between low and high active regime, the CO partial pressure is not uniform in the chamber and the temperature is not constant on the sample,[58] in particular CO oxidation reaction is strongly exothermic. These inhomogeneities, which could favor a transition by an hyperactive regime, are attenuated in our set-up since the sample heating is controlled with an IR pyrometer allowing to instantaneously adjust the power supplied in a more efficient way than with the usual thermocouple set-up.

The high active surface

The CO oxidation rates measured in the present study are closer to those reported on Pd(100) during coupled measurements of the reactivity and of the structure by *in situ* GIXRD, in a flow reactor.[23] The conversion rate reached a plateau at 200 CO_2 molecules.site^{-1}.s^{-1} for temperatures above 500K and for O_2/CO pressure ratio decreasing below ten. This rate is little less than 500 CO_2 molecules.site^{-1}.s^{-1} found at 470K in the present work when the O_2/CO pressure ratio reaches 100. The structure of the oxide layer formed under reactive conditions on Pd(100) strongly depends on this ratio, going from an almost perfect epitaxial thin layer, when it is near the stoichiometric value, to a thicker and more disordered oxide layer when the gas mixture is richer in oxygen. [23,59] A detailed study of the oscillation regime for high O_2/CO ratio shows the presence of epitaxial strained oxide grains and unstrained misaligned PdO grains during; the first ones would be dominant just after the transition and supposed to be the more active ones.[60] It is tempting to make the link with the strained oxide layer formed on $Au_{30}Pd_{70}$(110).

In the range of the O_2/CO pressure ratio where the strained oxide exists on $Au_{30}Pd_{70}$(110), the rate of CO_2 formation is directly correlated to a high reactive regime. It increases linearly with CO pressure, indicating that the reaction follows the Langmuir-Hinshelwood mechanism (CO adsorption and reaction) with a rate controlled by the CO adsorption that appears to be weak on this oxide surface. Such mechanism was predicted on the PdO(101) stoichiometric surface of the LP phase.[61] Moreover, the PdO strained phase is much more reactive under CO pressure than the usual oxide, since we showed that it is more easily reduced. Thus when CO is adsorbed on this strained PdO phase, it can readily react with the lattice oxygen atoms to produce CO_2 creating oxygen vacancies that can be refilled if the O_2/CO pressure ratio stays large enough.

Low reactive surface

When the O_2/CO pressure ratio goes down to the critical value, for instance 50 at 470K, the surface switches to a low active regime with a reaction rate not distinguishable from that produced by the sample environment in our experimental conditions. That corresponds to a reduced surface state with a thin layer of pure palladium poisoned by CO. A small expansion of the inter-planar spacing was measured similarly to what was already observed in the case of CO oxidation on Pd NPs and attributed to PdC_x phases.[62] A carbide phase has never been

observed previously for the low reactive surface on bulk Pd, but it can be favored on $Au_{30}Pd_{70}$ surface because of the intrinsic increase of the lattice parameter due to gold concentration. The whole expansion, of 2 % relatively to bulk Pd, measured for the reduced surface would correspond to a carbon concentration of about 13 %.[63] The cause of this carbide formation is not clear but it was predicted by a theoretical study showing that the CO disproportionation reaction (Boudouard reaction) can occur on palladium;[64] the possibility of such reaction on Au(110) surface was also proposed from PM-IRRAS observations.[65] From our data, we cannot definitively conclude that the low active regime is due to a PdC_x phase. Anyway, it cannot be attributed to the usual bulk-like PdO phase under ambient pressure, even in a polycrystalline form as deduced by X-ray diffraction results. Indeed, it was assumed that the relaxation from a strained PdO oxide to a powder-like layer would coexist with metallic palladium in the reduced phase and would be responsible for the switch to the low active phase in the case of CO oxidation on Pd(100).[60] Also, it was evidenced for the very specific case of the oscillating regime, where there is no indication of a role played by O_2/CO ratio, but rather by the roughness of the surface.[34] This results in the variation of the width of the oxide and surface peaks correlated to the oscillations. Here we observe in figure 12 that, in the frame of the accuracy of our measurements, the width of the surface peak stays constant during the different stages ((1x1), (1x2), "K=1") before the structural transition to a PdO surface layer. Regarding the oxide peak at the beginning of the growth, its width is larger testifying to smaller domains but its intensity increase corresponds to an enlargement of the lateral size of domains and to a thickening of the PdO layer (cf. Table 1); the limit being reached when the peak width tends toward the surface peak value (cf. figure 12).

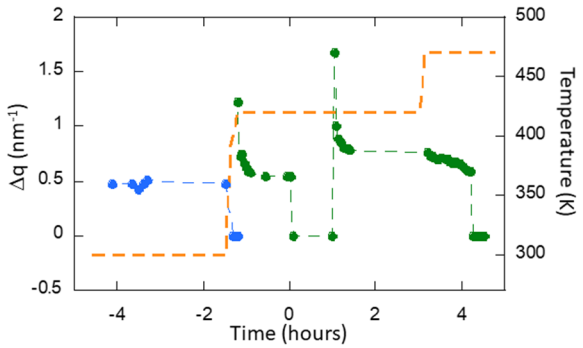

Figure 12 *: Δq variation of the (010) surface alloy peak (in blue), of the $(002)_{PdO}$ oxide peak at (0 1.47 0) (in dark green) and of the sample temperature (in orange) as a function of time in the same conditions as in figure 1.*

Gold effect on the activity

Regarding the influence of gold on the palladium activity, we did not observe any significant effect but our experimental conditions proved to be non-optimal to achieve such an information. The first reason is the sensitivity of our experimental setup. Indeed AuPd(100) activity was large compared to Pd(110) in the temperature range where it is limited by CO poisoning, but it never exceeds 100 CO_2 molecules.site^{-1}.s^{-1}.[10] Moreover, in the case of AuPd mixed surface where the active sites are only Pd atoms, the total activity is much lower and more difficult to detect. A second obstacle in highlighting a gold-palladium synergistic effect is the narrowness of the range where a mixed Au-Pd surface is stabilized on $Au_{30}Pd_{70}$(110), since CO and oxygen pressures both induce palladium segregation. We observed a mixed gold-palladium surface under 500 mbar O_2 added to 1 mbar CO at room temperature with no detectable reaction. When increasing the temperature the surface quickly became pure palladium and thus probably CO poisoned. However we were able to grow an almost perfect oxide layer on $Au_{30}Pd_{70}$(110) unlike on pure palladium crystal where the oxide layer is desordered and its structural as well as catalytic properties are difficult to characterize. Thus, there is no direct synergistic effect between gold and palladium on the catalytic properties for $Au_{30}Pd_{70}$(110) but it creates the conditions for the growth of a highly reactive palladium oxide phase.

Conclusion

This study on $Au_{30}Pd_{70}$(110) correlated the surface composition and the depth profile of its structure to its catalytic properties for CO oxidation under semi-realistic reaction conditions, with oxygen rich pressure and at moderate temperatures (300 to 470K). It also brought a new insight into the mechanism of the CO oxidation reaction on pure palladium surfaces.

After preparation the surface is (1x1) and pure gold. Pure oxygen or pure CO pressure induce Pd segregation towards the surface, even at room temperature, with a missing row reconstruction under O_2 and terrace or surface roughness under CO.

When increasing pressure of O_2 or under CO+O_2 mixture – with the pressure O_2/CO ratio above a critical value allowing to overcome CO poisoning – a precursor state is observed

before structural change to palladium oxide. During this stage, the 3 topmost planes are Pd enriched with expansion attributed to oxygen dissolution in the subsurface region. This structure can be correlated to the “complex” structure observed on Pd(110) surface.

Then a strained phase of PdO grows on the alloy in the $[100]_{PdO}$ direction from about 400 K and forms a thin layer of a few ML (less than a dozen atomic planes) above a buffer layer (2 or 3 monolayers) gold enriched and in registry with the underneath alloy.

The Bragg peaks of this strained PdO phase do not coincide with that of the $P4_2/mmc$ structure of PdO bulk usually observed under ambient conditions. It is rather consistent with the high pressure I4/mmm PdO structure strained by epitaxy on the underneath alloy and would relax to the usual PdO structure for higher oxidizing conditions and layer thickness.

The strained PdO layer is more easily reduced by CO than the usual PdO phase and it is correlated to a high activity for CO oxidation whereas the reduced surface is lowly active. The high reactive regime follows the Langmuir-Hinshelwood mechanism (CO adsorption and reaction) with a rate controlled by the CO adsorption.

In the frame of the accuracy of our experiments we did not detect any enhancement of the catalytic activity due to a synergetic effect between gold and palladium. Moreover we showed that both CO and oxygen induce Pd segregation towards the surface even at room temperature. However, alloying with gold seems to play a significant role in the growth of the PdO layer slowing down the oxygen dissolution. This yields the formation of a relatively well defined thin layer of a strained phase of PdO allowing to properly identifying it and to measure its reactivity.

Finally, we stress that this PdO strained layer, grown on $Au_{30}Pd_{70}(110)$ surface, can reach a very high CO conversion rate into CO_2 at moderate temperature (470K). Moreover several results tend to prove that this well ordered layer is representative of what happens on pure Pd(110) surface. It would thus be interesting to investigate faces (100) and (111) to compare them to the (110), since all these faces present similarity between the surface oxides and the chemisorbed oxygen from a viewpoint of availability of active oxygen.[66] Further work is needed to fully determine the structure of this high active phase especially to understand the origin of the extra diffraction peak not allowed by the symmetry of the previously known PdO structures. In particular, it could be helpful to complete our approach with near ambient

pressure XPS. Such study on $Au_{30}Pd_{70}$(110) surface is under progress to confirm the key role of the strained PdO structure in this highly interesting gold and palladium based system for catalysis under mild conditions.

Acknowledgement: The authors thank the technical staff (SERAS) of Institut Néel CNRS and of the BM32 CRG beamline at ESRF, in particular O. Ulrich, for their valuable help.

References

(1) M. Haruta, M.; Kobayashi, T.; Sano, H.; Yamada, N. Gold Catalysts Prepared by Co-precipitation for Low-Temperature Oxidation of Hydrogen and of Carbon Monoxide. *J. Catal.* **1989**, *115*, 301-309.

(2) Chen, M.; Goodman, D. W. Catalytically Active Gold: From Nanoparticles to Ultrathin Films. *Acc. Chem. Res.* **2006**, *39*, 739−746

(3) Schubert, M. M.; Hackenberg, S.; van Veen, A. C.; Muhler, M.; Plzak, V.; Behm R. J. CO Oxidation over Supported Gold Catalysts—"Inert" and "Active" Support Materials and Their Role for the Oxygen Supply during Reaction. *J. Catal.* **2001**, *197*, 113–122.

(4) Green, I. X.; Tang, W.; Neurock, M.; Yates. M. J. T. Jr. Spectroscopic Observation of Dual Catalytic Sites During Oxidation of CO on a Au/TiO_2 Catalyst. *Science* **2011,** *333*, 736−739.

(5) Saint-Lager, M.-C. ; Laoufi, I. ; Bailly A. Operando atomic structure and active sites of TiO_2(110)-supported gold nanoparticles during carbon monoxide oxidation, *Faraday Discuss.* **2013**, *162*, 179-190.

(6) Valden, M.; Lai, X.; Goodman D. W. Onset of Catalytic Activity of Gold Clusters on Titania with the Appearance of Nonmetallic Properties. *Science* **1998**, *281*, 1647–1650.

(7) Laoufi, I.; Saint−Lager, M.-C.; Lazzari, R.; Jupille, J.; Robach, O.; Garaudée, S.; Cabailh, G.; Dolle, P.; Cruguel H.; Bailly A. Size and catalytic activity of supported gold nanoparticles: an in operando study during CO oxidation. *J. Phys. Chem. C* **2011** *115*, 4673-4679.

(8) Engel, T.; Ertl, G. Elementary Steps in the Catalytic Oxidation of Carbon Monoxide on Platinum Metals. *Adv. Catal.* **1979**, *28*, 1–78**.**

(9) Berlowitz, P. J.; Peden, C. H. F.; Goodman D. W. Kinetics of CO Oxidation on Single-Crystal Pd, Pt, and Ir. *J. Phys. Chem* **1988**, *92*, 5213-5221.

(10) Gao, F.; Wang, Y.; Goodman, D. W. CO oxidation over AuPd(100) from ultrahigh vacuum to near-atmospheric pressures: CO adsorption-induced surface segregation and reaction kinetics. *J. Phys. Chem. C* **2009**, *113*, 14993–15000.

(11) Gao, F.; Wang, Y.; Goodman, D. W. CO oxidation over AuPd(100) from ultrahigh vacuum to near-atmospheric pressures: the critical role of contiguous Pd atoms. *J. Am. Chem. Soc.* **2009**, *131*, 5734–5735.

(12) Gao, F.; Wang, Y.; Goodman, D. W. Reaction kinetics and polarization-modulation infrared reflection absorption spectroscopy (PM-IRAS) investigation of CO oxidation over supported Pd-Au alloy catalysts. *J. Phys. Chem. C* **2010**, 114, 4036–4043.

(13) Gao, F.; Goodman D. W. Pd–Au bimetallic catalysts: understanding alloy effects from planar models and (supported) nanoparticles. *Chem. Soc. Rev.* **2012**, 41, 8009–8020.

(14) Kuntze, J.; Speller, S.; Heiland, W.; Atrei, A.; Rovida, G.; Bardi, U. Surface structure and composition of the alloy $Au_3Pd(100)$ determined by LEED and ion scattering spectroscopy. *Phys. Rev. B* **1999**, *60*, 1535–1538.

(15) J. Kuntze, S. Speller, W. Heiland, P. Deurinck, C. Creemers, A. Atrei, U. Bardi. Surface structure and segregation profile of the alloy $Au_3Pd(110)$: Experiment and theory. *Phys. Rev. B* **1999**, 60, 9010–9018.

(16) Bailly, A. Surfaces modèles or-palladium étudiées in situ : de l'ultra-vide aux conditions de réactions catalytiques, PhD Thesis, Université Joseph Fourier Grenoble 1, 2005, https://tel.archives-ouvertes.fr/tel-00011720.

(17) Languille, M.-A. « Etude in situ de surfaces monocristallines Au et Pd-Au. Absorption du CO et de O_2. *PhD Thesis n°38/2008*, University Claude Bernard Lyon 1, 2008.

(18) Languille, M. A.; Ehret, E.; Lee, H. C.; Jeong, C. K.; Toyoshima, R.; Kondoh, H.; Mase, K.; Jugnet, Y.; Bertolini, J.-C.; Aires, F. J. C. S.; Mun, B. S. In-situ surface analysis of AuPd(110) under elevated pressure of CO. *Catal. Today* **2016**, *260*, 39–45.

(19) Saint-Lager, M.-C.; Languille, M.-A.; Cadete Santos Aires, F. J.; Bailly, A.; Garaudée, S.; Ehret E.; Robach, O. Oxygen-induced changes of the $Au_{30}Pd_{70}(110)$ surface structure and composition under increasing O_2 pressure, *J. Phys. Chem. C*, 2018, *122*, 22588–2259.

(20) Delannoy, L.; Giorgio, S.; Mattei, J. G.; Henry, C. R.;. El Kolli, N; Méthivier, C.; Louis, C. Surface segregation of Pd from TiO_2-supported AuPd nanoalloys under CO oxidation conditions observed in situ by ETEM and DRIFTS. *ChemCatChem* **2013**, *5*, 2707–2716.

(21) Mars, P.; Van Krevelen D.W. Oxidations carried out by means of vanadium oxide catalysts, *Chem. Eng. Sci.* **1954** , *3*, 41–59.

(22) Hendriksen, B. L. M.; Bobaru, S.C.; Frenken J. W. M. Oscillatory CO oxidation on Pd(1 0 0) studied with in situ scanning tunneling microscopy. *Surf. Sci.* **2004**, *552*, 229–242.

(23) Van Rijn, R. ; Balmes, O.; Resta, A.; Wermeille, D.; Westerström, R.; Gustafson, J.; Felici, R.; Lundgren, E.; Frenken J.W.M. Surface structure and reactivity of Pd(100) during CO oxidation near ambient pressures. *Phys. Chem. Chem. Phys.* **2011**, *13*, 13167–13171.

(24) Van Spronsen, M. A.; Frenken, J. W. M.; Groot I. M. N. Surface science under reaction conditions: CO oxidation on Pt and Pd model catalysts. *Chem. Soc. Rev.* **2017**, *46*, 4347-4374.

(25) Chen, M.S.; Cai, Y.; Yan, Z.; Gath K.K.; Axnanda, S.; Goodman D.W. Highly active surfaces for CO oxidation on Rh, Pd, and Pt. *Surf. Sci.* **2007***, 601*, 5326–5331.

(26) Gao, F.; McClure, S. M.; Cai, Y.; Gath, K. K.; Wang, Y.; Chen, M. S.; Guo, Q. M.; Goodman, D. W. CO oxidation trends on Pt-group metals from ultrahigh vacuum to near atmospheric pressures: a combined in situ PM-IRAS and reaction kinetics study. *Surf. Sci.* **2009**, *603*, 65–70.

(27) Gao, F. ; Wang, Y. L.; Goodman D. W. CO oxidation trends on Pt-group metals from ultrahigh vacuum to near atmospheric pressures: a combined in situ PM-IRAS and reaction kinetics study. *J. Phys. Chem. C* **2010**, *114*, 4036 –4043.

(28) Chen, M. ; Zheng, Y.; Wan H. Kinetics and Active Surfaces for CO Oxidation on Pt-Group Metals Under Oxygen Rich Conditions. *Top Catal.* **2013**, *56*, 1299–1313.

(29) Saint-Lager, M.-C.; Bailly, A.; Dolle, P.; Baudoing-Savois, R.; Taunier, P.; Garaudée, S.; Cuccaro, S.; Douillet, S.; Geaymond, O.; Perroux, G. *et al.* New reactor dedicated to *in operando* studies of model catalysts by means of surface x-ray diffraction and grazing incidence small angle x-ray scattering. *Rev. Sci. Instrum.* **2007**, *78*, 083902–083910.

(30) Vlieg, E. Integrated intensities using a six-circle surface X-ray diffractometer. *J. Appl. Cryst*. **1997**, *30*, 532–543.

(31) Vlieg, E. ROD: a program for surface X-ray crystallography. *J. Appl. Crystallogr*. **2000**, *33*, 401–405.

(32) Robinson, I.K. Crystal truncation rods and surface roughness. *Phys. Rev. B* **1986**, *33*, 3830–3836.

(33) Hendriksen, B. M.; Ackermann, M. D.; Van Rijn, R.; Stoltz, D.; Popa, I.; Balmès, O.; Resta, A.; Wermeille, D.; Felici, R.; Ferrer, S.; Frenken J. W. M. The role of steps in surface catalysis and reaction oscillations. *Nat. Chem.* **2010**, *2*, 730-734.

(34) Thostrup, P.; Christoffersen, E.; Lorensen, H.T.; Jacobsen, K.W.; Besenbacher, F.; Nørskov J. K. Adsorption-induced step formation. *Phys. Rev. Lett.* **2001**, *87*, 126102.

(35) Weschke, E.; Schüßler-Langeheine, C.; Meier, R.; Kaindl, G. ; Sutter, C.; Abernathy, D.; Grübel G. *q* Dependence of the Growth-Oscillation Period of X-Ray Reflectivity in Heteroepitaxy: Ho/W(110)**.** *Phys. Rev. Lett.* **1997**, *79*, 3954-3957.

(36) Han, J.; Zemlyanov, D. Y.; Ribeiro F. H. Interaction of O2 with Pd single crystals in the range 1–150 Torr: Surface morphology transformations. *Surf. Sci.* **2006**, *600*, 2730–2744.

(37) Zemlyanov, D.; Klötzer B.; Gabasch, H.; Smeltz, A.; Ribeiro, F. H.; Zafeiratos, S.; Teschner, D.; Schnörch, P.; Vass, E.; Hävecker M. *et al.* Kinetics of Palladium Oxidation in the mbar Pressure Range: Ambient Pressure XPS Study. *Top Catal.* **2013**, *56*, 885–895.

(38) Lundgren, E.; Kresse, G.; Klein, C.; Borg, M.; Andersen, J. N.; De Santis, M.; Gauthier, Y.; Konvicka, C.; Schmid, M.; Varga P. Two-Dimensional Oxide on Pd(111). *Phys. Rev. B* **2002**, *88*, 246103.

(39) Zemlyanov, D. ; Aszalos-Kiss, B.; Kleimenov, E.; Teschner, D.; Zafeiratos, S.; Hâvecker, M.; Knop-Gericke, A.; Schlögl, R.; Gabasch, H.; Unterberger, W. *et al.* In situ XPS study of Pd(111) oxidation. Part 1: 2D oxide formation in 10^{-3} mbar O_2 *Surf. Sci.* **2006**, *600*, 983–994.

(40) Han, J. ;. Zemlyanov, D. Y; Ribeiro F. H. Interaction of O2 with Pd single crystals in the range 1–150 Torr: Oxygen dissolution and reaction. *Surf. Sci.* **2006**, *600*, 2752-2761

(41) Westerström, R.; Weststrate, C. J.; Resta, A.; Mikkelsen, A.; Schnadt, J.; Andersen, J. N.; Lundgren, E.; Schmid, M.; Seriani, N.; Harl, J. *et al.*Stressing Pd atoms: Initial oxidation of the Pd(110) surface. *Surf. Sci.* **2008**, *602*, 2440–2447.

(42) G. Ertl, P. Rau. Chemisorption und katalytische reaktion von sauerstoff und kohlenmonoid an ainer palladium (110)-oberfläche. *Surf. Sci.* **1969**, *15*, 443–465.

(43) Westerström, R.; Weststrate, C. J.; Gustafson, J.; Mikkelsen, A.; Schnadt, J.; Andersen, J. N.; Lundgren, E.; Seriani, N.; Mittendorfer, F.; Kresse, G.; Stierle, A. Lack of surface oxide layers and facile bulk oxide formation on Pd(110). *Phys. Rev. B* **2009**, *80*, 125431.

(44) Todorova, M.; Reuter, K.; Scheffler M. Density-functional theory study of the initial oxygen incorporation in Pd(111). *Phys. Rev. B* **2005**, *71*, 195403 1-8.

(45) Vattuone, L.; Gerbi, A.; Cappelletti, D.; Pirani, F.; Gunnella, R.; Savio, L.; Rocca M. Selective Production of Reactive and Nonreactive Oxygen Atoms on Pd(001) by Rotationally Aligned Oxygen Molecules. *Angew. Chem. Int. Ed.* **2009**, *48*, 4845-4848.

(46) Rose, M. K.; Borg, A.; Mitsui, T.; Ogletree, D. F.; Salmeron M. Subsurface impurities in Pd(111) studied by scanning tunneling microscopy. *J. Chem. Phys.* **2001**, *115,* 10928-10934.

(47) Lundgren, E. ; Gustafson, J.; Mikkelsen, A.; Andersen, J. N.; Stierle A.; Dosch, H.; Todorova, M.; Rogal, J.; Reuter, K.; Scheffler M. Kinetic Hindrance during the Initial Oxidation of Pd(100) at Ambient Pressures. *Phys. Rev. B* **2004**, *92*, 046101 1-4

(48) Gustafson, J.; Shipilin, M.; Zhang, C.; Stierle, A.; Hejral, U.; Ruett, U.; Gutowski, O.; Carlsson, P.-A.; Skoglundh, M.; Lundgren E. High-energy surface X-ray diffraction for fast surface structure determination. *Science* **2014**, *343*, 758−761.

(49) Waser J. The Structure of PdO. *Acta Cryst.* **1953**, *6*, 661-663

(50) Rogers, D.; Shannon, R.; Gillson J. Crystal Growth and Semi-conductivity of Palladium Oxide. *J. Solid State Chem.* **1971**, *3*,314-316

(51) Gmelin Handbook of Inorganic and Organometallic Chemistry, 8th ed.; Pd compounds Suppl. B2; Griffith, W. P., Swars, K.; et al., Eds.; Springer: Berlin, 1989.

(52) Christy, A. G.; Clarck S.M. Structural behavior of palladium (II) oxide and a palladium suboxide at high pressure: an energy-dispersive x-ray-diffraction study. *Phys. Rev. B* **1995**, *13*, 9259-9265.

(53) van Rijn, R.; Balmes, O.; Resta, A.; Wermeille, D.; Westerström, R.; Gustafson, J.; Felici, R.; Lundgren, E.; Frenken, J. W. M. Surface structure and reactivity of Pd(100) during CO oxidation near ambient pressures. *Phys. Chem. Chem. Phys.* **2011**, 13, 13167−13171.

(54) Kasper, N.; Nolte, P.; Stierle A. Stability of Surface and Bulk Oxides on Pd(111) Revisited by in Situ X-ray Diffraction. *J. Phys. Chem. C* **2012**, *116*, 21459−21464.

(55) Rogal, J.; Reuter, K.; Scheffler M. Thermodynamic stability of PdO surfaces. *Phys. Rev. B* **2004**, *69*, 075421 1-8.

(56) Penner S.; Wang, D.; Jenewein, B.; Gabasch, H.; Klötzer, B.; Knop-Gericke, A.; Schlögl, R.; Hayek, K. Growth and decomposition of aligned and ordered PdO nanoparticles. *J. Chem. Phys.* **2006**, *125*, 094703.

(57) Gabasch, H.; Knop-Gericke, A.; Schlögl, R.; Borasio, M.; Weilach, C.; Rupprechter, G.; Penner, S.; Jenewein, B.; Hayek K.; Klötzer B. Comparison of the reactivity of different Pd–O species in CO oxidation. *Phys. Chem. Chem. Phys.* **2007**, *9*, 533-540.

(58) Blomberg, S.; Brackmann, C.; Gustafson, J.; Aldén, M.; Lundgren, E.; Zetterberg J. Real-Time Gas-Phase Imaging over a Pd(110) Catalyst during CO Oxidation by Means of Planar Laser-Induced Fluorescence. *ACS Catal*. **2015**, *5*, 2028−2034.

(59) Shipilin, M. ; Gustafson, J.; Chu, Z.; Merte, L. R.; Stierle, A.; Hejral, U.; Ruett, U.; Gutowski, O.; Skoglundh, M.; Carlsson, P.-A.; Lundgren E. Transient Structures of PdO during CO Oxidation over Pd(1 0 0). *J Phys Chem* C. **2015**, *119*, 15469–15476.

(60) Onderwaater, W.G.; Balmès, O; Roobol, S.B.; van Spronsen, M.; Drnec, J.; Carla, F.; Felici, R.; Frenken, J. W. M. Oxidation of CO on Pd(100): on the structural evolution of the PdO layer during the self sustained oscillation regime. *Catal. Struct. React.* **2017**, *3*, 89–94.

(61) Hirvi, J. T.; Kinnunen, T. J. J.; Suvanto, M.; Pakkanen, T. A.; Norskov, J. K. J. CO oxidation on PdO surfaces *Chem. Phys.* **2010**, *133*, 084704.

(62) Balmes, O.; Resta, A.; Wermeille, D. ; Felici, R.; Messing, M. E.; Deppert, K.; Liu, Z.; Grass, M. E.; Bluhm, H.; van Rijn, R. *et al*. Reversible formation of a PdCx phase in Pd nanoparticles upon CO and O_2 exposure *Phys. Chem. Chem. Phys.,* **2012**, *14*, 4796–4801.

(63) Maciejewski, M.; Baiker A. Incorporation of Carbon into Palladium during Low-Temperature Disproportionation of CO over Pd/ZrO_2 Prepared from Glassy Pd-Zr Alloys. *J. Phys. Chem.* **1994***, 98,* 285

(64) Sautet, P.; Cinquini F. Surface of Metallic Catalysts under a Pressure of Hydrocarbon Molecules: Metal or Carbide? *ChemCatChem,* **2010**, *2*, 636–639.

(65) Jugnet, Y.; Cadete Santos Aires, F. J.; Deranlot, C.; Piccolo, L.; Bertolini J.- C. CO chemisorption on Au(110) investigated under elevated pressures by polarized reflection absorption infrared spectroscopy and scanning tunneling microscopy Surface Science **2002**, *521*, L639-L644.

(66) Kondoh, H. ; Toyoshima, R.; Monya, Y.; Yoshida, M.; Mase, K.; Amemiya, K.; Mun B. S. In situ analysis of catalytically active Pd surfaces for CO oxidation with near ambient pressure XPS. *Catalysis Today,* **2016***, 260*, 14–20.

Table of Contents (TOC) graphics